

SUPPLEMENTARY INFORMATION

BCN Monolayer for High Capacity Al based Dual-Ion Batteries

Hariom Saini^a, Sandeep Das^a and Biswarup Pathak^{a*}

^aDiscipline of Chemistry, Indian Institute of Technology (IIT) Indore, Simrol, Indore 453552, India

*Email: biswarup@iiti.ac.in

Contents

Fig. S1 Total energy vs time plot for AIMD simulations of the BCN monolayer at (a) 300 K and (b) 400 K. The side and top views of (c) initial structure (d) structure after 20 ps simulation at 300 K and (e) 400 K.

Fig. S2 Top view of the AlCl_4 adsorbed BCN monolayer at (a) B Top, (b) C Top, (c) N Top, (d) B-C Bridge, (e) B-N Bridge, (f) C-N Bridge, (g) C-C Bridge, (h) C-C-B-N-B-N Hollow and (i) C-B-N-C-B-N Hollow sites.

Table S1 The relative adsorption energy of AlCl_4 for all possible adsorption sites available and the average distance of Al of the adsorbed AlCl_4 from BCN monolayer at each site.

Fig. S3 Side and top views of the most stable configuration of AlCl_4 adsorbed BCN monolayer at different AlCl_4 concentrations (a) $(\text{AlCl}_4)_4\text{BCN}$ (b) $(\text{AlCl}_4)_8\text{BCN}$ (c) $(\text{AlCl}_4)_{12}\text{BCN}$.

Fig. S4 Top view of the optimized configuration of 15 AlCl_4 adsorbed BCN monolayer. Inset figure showing side view of AlCl_4 dissociation.

Fig. S5 Total and partial density of states of (a) 7 AlCl_4 adsorbed BCN monolayer, (b) 10 AlCl_4 adsorbed BCN monolayer, (c) 14 AlCl_4 adsorbed BCN monolayer. The Fermi level is set at zero.

Fig. S6 The optimized highest energy transition states for different possible pathways, (a) Path A, (b) Path B, (c) Path C, available for AlCl_4 diffusion.

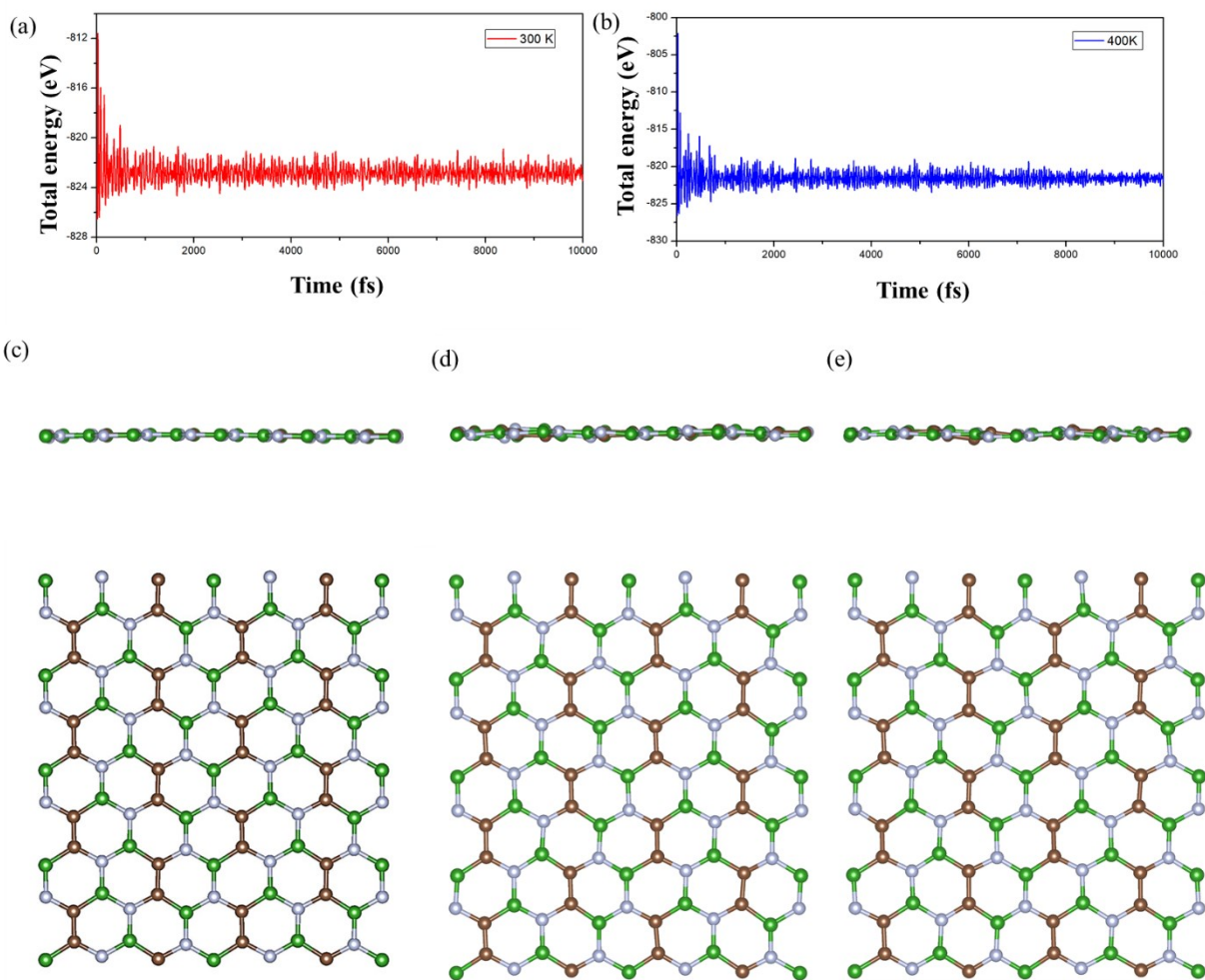


Fig. S1 Total energy vs time plot for AIMD simulations of the BCN monolayer at (a) 300 K and (b) 400 K. The side and top views of (c) initial structure (d) structure after 20 ps simulation at 300 K and (e) at 400 K.

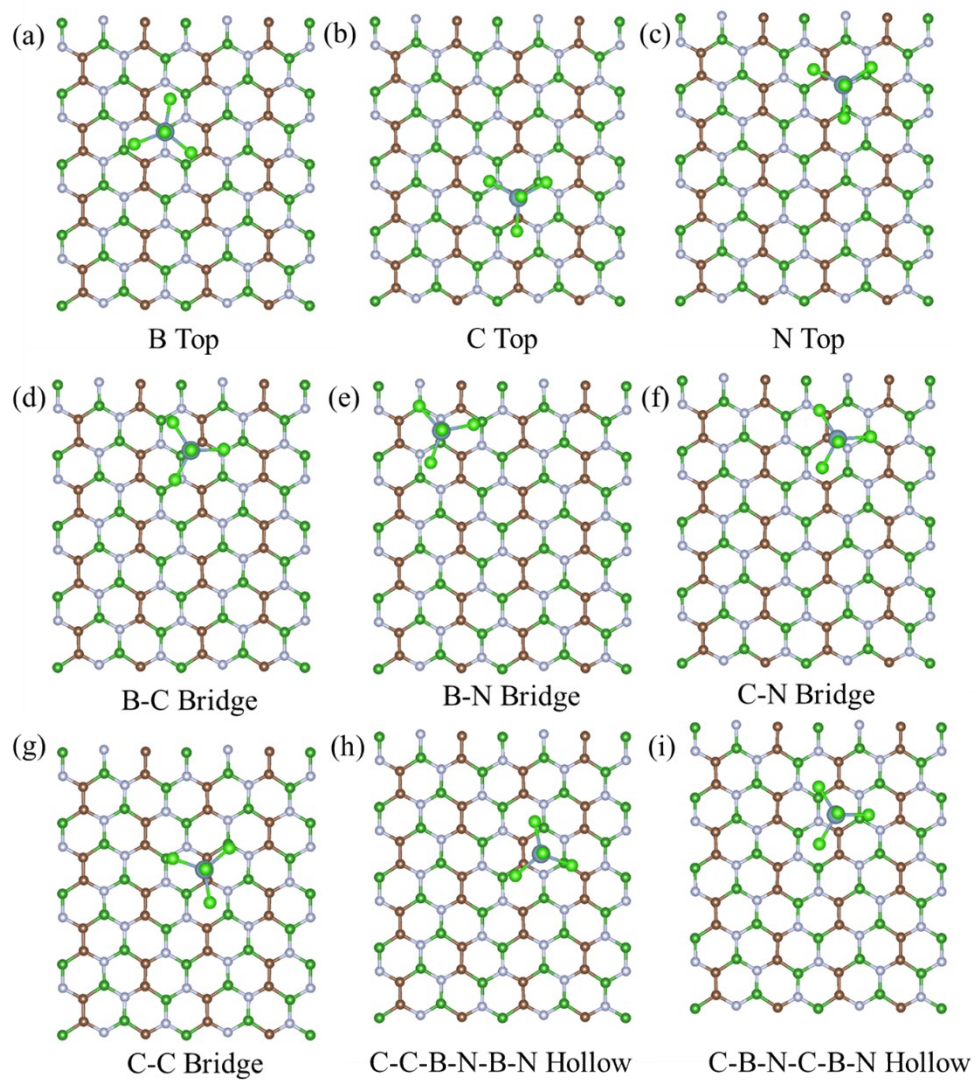


Fig. S2 Top view of the AlCl_4 adsorbed BCN monolayer at (a) B Top, (b) C Top, (c) N Top, (d) B-C Bridge, (e) B-N Bridge, (f) C-N Bridge, (g) C-C Bridge, (h) C-C-B-N-B-N Hollow and (i) C-B-N-C-B-N Hollow sites.

Table S1 The relative adsorption energy of AlCl_4 for all possible adsorption sites available and the average distance of Al of the adsorbed AlCl_4 from BCN monolayer at each site.

Sites		Relative Adsorption energy (eV)	Average Distance (\AA)
1	B Top	0.03	3.91
2	C Top	0.02	3.88
3	N Top	0.04	3.97
4	B-C Bridge	0.06	3.88
5	B-N Bridge	0.02	3.93
6	C-N Bridge	0.03	3.89
7	C-C Bridge	0.01	3.87
8	C-C-B-N-B-N Hollow	0.00	3.85
9	C-B-N-C-B-N Hollow	0.03	3.90

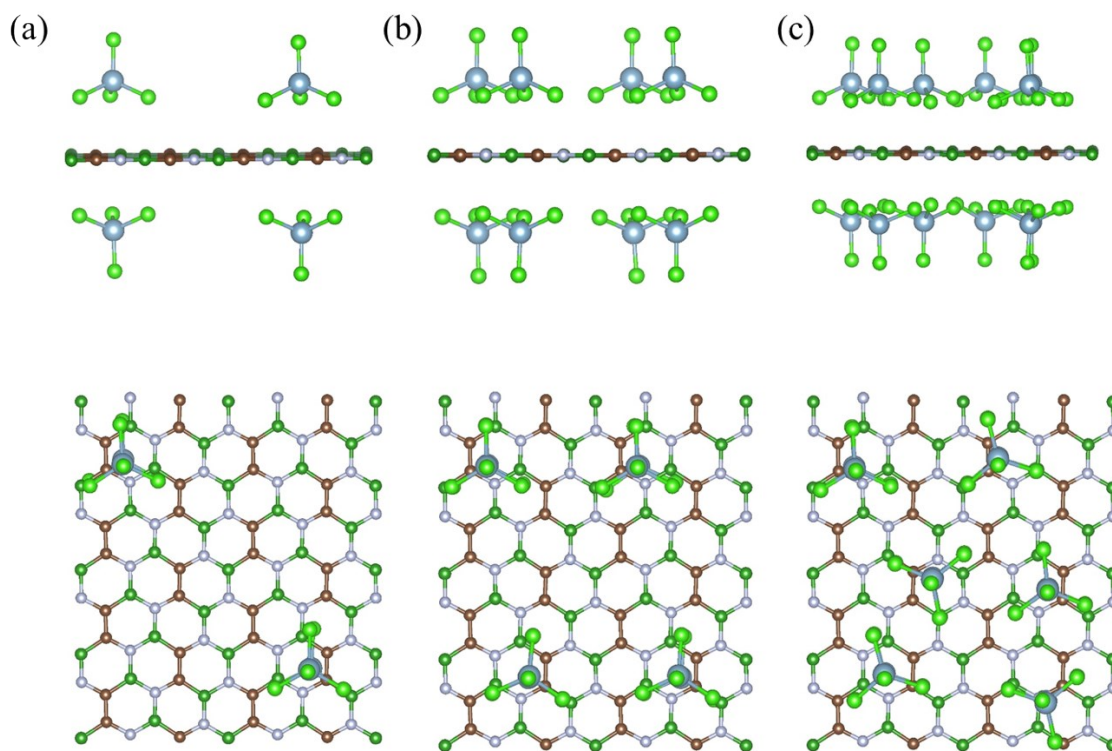


Fig. S3 Side and top views of the most stable configuration of AlCl_4 adsorbed BCN monolayer at different AlCl_4 concentrations (a) $(\text{AlCl}_4)_4\text{BCN}$ (b) $(\text{AlCl}_4)_8\text{BCN}$ (c) $(\text{AlCl}_4)_{12}\text{BCN}$.

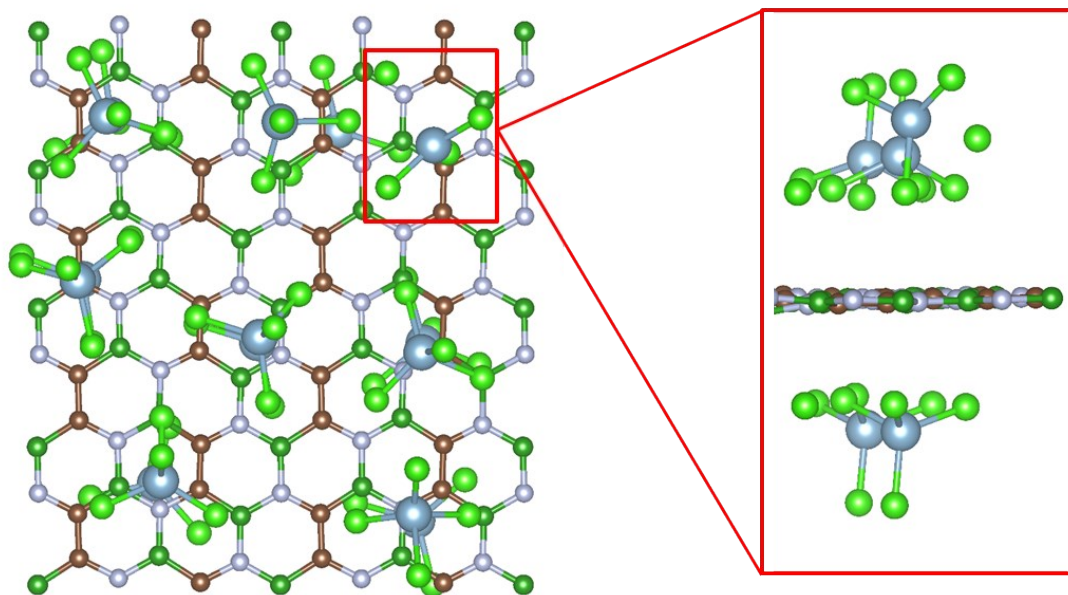


Fig. S4 Top view of the optimized configuration of 15 AlCl_4 absorbed BCN monolayer. Inset figure showing side view of AlCl_4 dissociation.

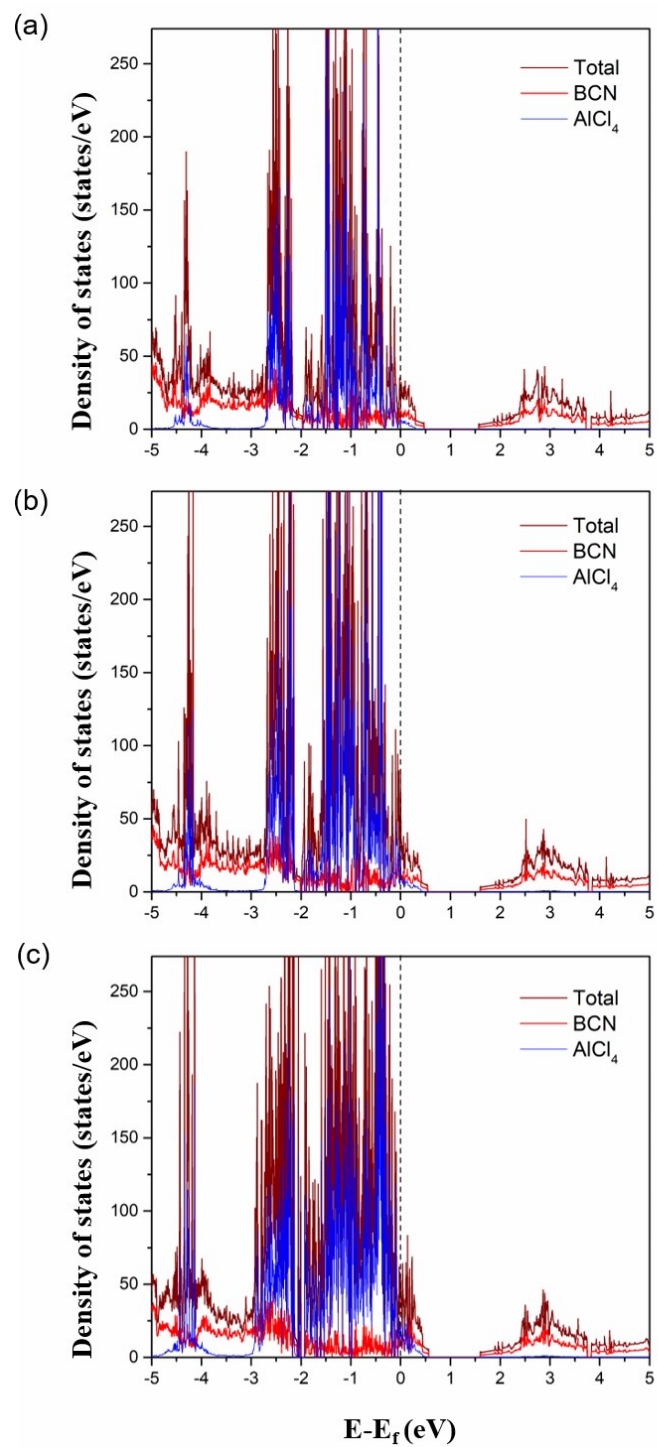


Fig. S5 Total and partial density of states of (a) 7 AlCl_4 adsorbed BCN monolayer, (b) 10 AlCl_4 adsorbed BCN monolayer, (c) 14 AlCl_4 adsorbed BCN monolayer. The Fermi level is set at zero.

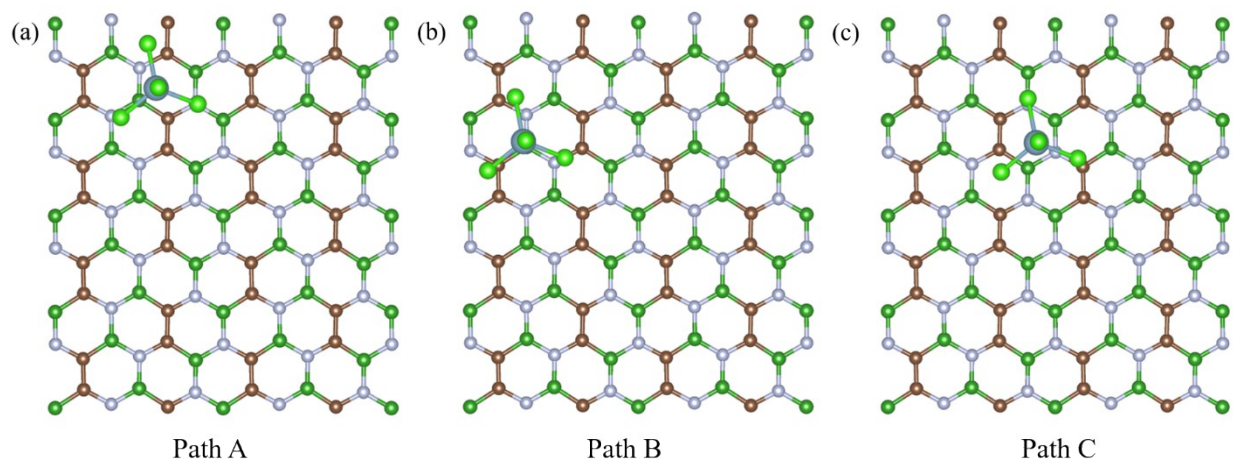


Fig. S6 The optimized highest energy transition states for different possible pathways, (a) Path A, (b) Path B, (c) Path C, available for AlCl_4 diffusion.